Biochimica et Biophysica Acta, 554 (1979) 1—22

BBA 78389

THREE DIMENSIONAL MICROSCOPIC SURFACE PROFILES OF MEMBRANES RECONSTRUCTED FROM FREEZE ETCHING ELECTRON MICROGRAPHS

R. KRBECEK, C. GEBHARDT, H. GRULER and E. SACKMANN

Universität Ulm, Abt. Experimentalphysik III, Oberer Eselsberg, D-7900 Ulm (F.R.G.)

(Received August 11th, 1978)
(Revised manuscript received December 27th, 1978)

Key words: Membrane structure; Phase separation; Membrane protein; Picture analysis; (Electron microscopy)

Summary

A method of three-dimensional reconstruction of the surface profile of artificial and natural membranes from freeze quenched electron micrographs is presented. The method is based on the analysis of the variation in thickness of platinum layers, deposited under an oblique angle. In essence, it is reminiscent of the method of Eratosthenes to measure the earth's radius. The thickness of etch-like protrusions of membranes could be determined to an accuracy of about 3 Å. True distances on curved surfaces rather than projections of distances are obtained. The method has been applied to both model membranes and biological membranes. The essential results are:

1. Detailed information on the symmetry and the molecular structure of the crystalline phases of dimyristoyl phosphatidylcholine was obtained. The microscopic surface profile of the ripple structure observed between the pretransition and the main transition was analysed. In accordance with a previous model we found that the ripple structure is caused by the spontaneous curvature of the monolayers. The surface profiles of the ripple structure and of the low temperature biaxial phase could be clearly distinguished.

2. The sizes and shapes of lipid domains formed by both thermically and charge-induced lateral phase separation were determined. This showed that the visual inspection of electron micrographs may lead to a considerable underestimation of the domain size. Conclusions may be drawn concerning the different phases formed upon lateral phase separation.

3. As a biological example, yeast cell membranes were studied. The method allows one to distinguish between different membrane-bound proteins by measuring the width-to-height ratio of the particles. The deformation of the lipid layer in the environment of the proteins may be determined. This deformation

contains information about lipid-mediated long-range interactions between membrane proteins.

Introduction

In transmission electron microscopy one obtains three dimensional pictures only if stereoscopic techniques are applied [1]. The scanning electron microscope [2] allows the production of three-dimensional pictures, but the resolution is rather low (c.f. Ref. 2, page 3). The freeze quenching technique preserves the natural structure of biological objects to a very large extent provided the freezing process is performed very rapidly. Pictures made from freeze etched objects contain the information of the three-dimensional structure in a latent form if the objects are shadowed under an oblique angle. The freeze etching technique can provide information only on those structural features of an object which affect its surface curvature. The primary purpose of the present paper is to present a method of three-dimensional reconstruction of the the surface profile of artificial and biological membranes. Information about the surface structure is gained by analysing the thickness of the metal layer deposited under an oblique angle. The principle of the method is illustrated in Fig. 1 *. In principle the technique is a modification of the famous method of Eratosthenes [3] who determined the curvature of the earth from the difference in the shadow lengths, measured simultaneously at two different locations.

Materials and Methods

Materials. Phospholipids were obtained from Fluka and were used without further purification. Baker's yeast cells were a gift from the 'Sektion Elektronenmikroskopie' of this University. Polylysine was a product of Miles Company with a molecular weight of 30 000.

Vesicle preparation. Large bilayer vesicles were prepared as described previously [4]. First, thin layers of the lipid or the lipid mixture were deposited on the bottom of an Erlenmeyer flask. Then water was poured gently over the lipid layers. Large, single walled vesicles formed spontaneously.

Freeze quenching procedure. The samples were frozen in two ways. In the first method (slow cooling procedure), the samples were transfered into cold Freon of −155°C for about 3 s. They were then stored in liquid nitrogen before use. The cooling rate was of the order of 10^2 degrees · s^{-1}. Secondly, a spraying technique was applied (fast cooling procedure) [5]. Small droplets (about 10 μm diameter) of the preparation under study were shot into liquid propane kept at −190°C. For that purpose a sprayer driven by compressed air was used. After evaporation of the refrigerant the frozen droplets were taken up in butylbenzene at −85°C. These specimens were deposited on precooled gold plates and stored in liquid nitrogen. The cooling rate was estimated as

* Preliminary results were presented at the 5th International Conference on Electron Microscopy, Münster, F.R.G., 1977.

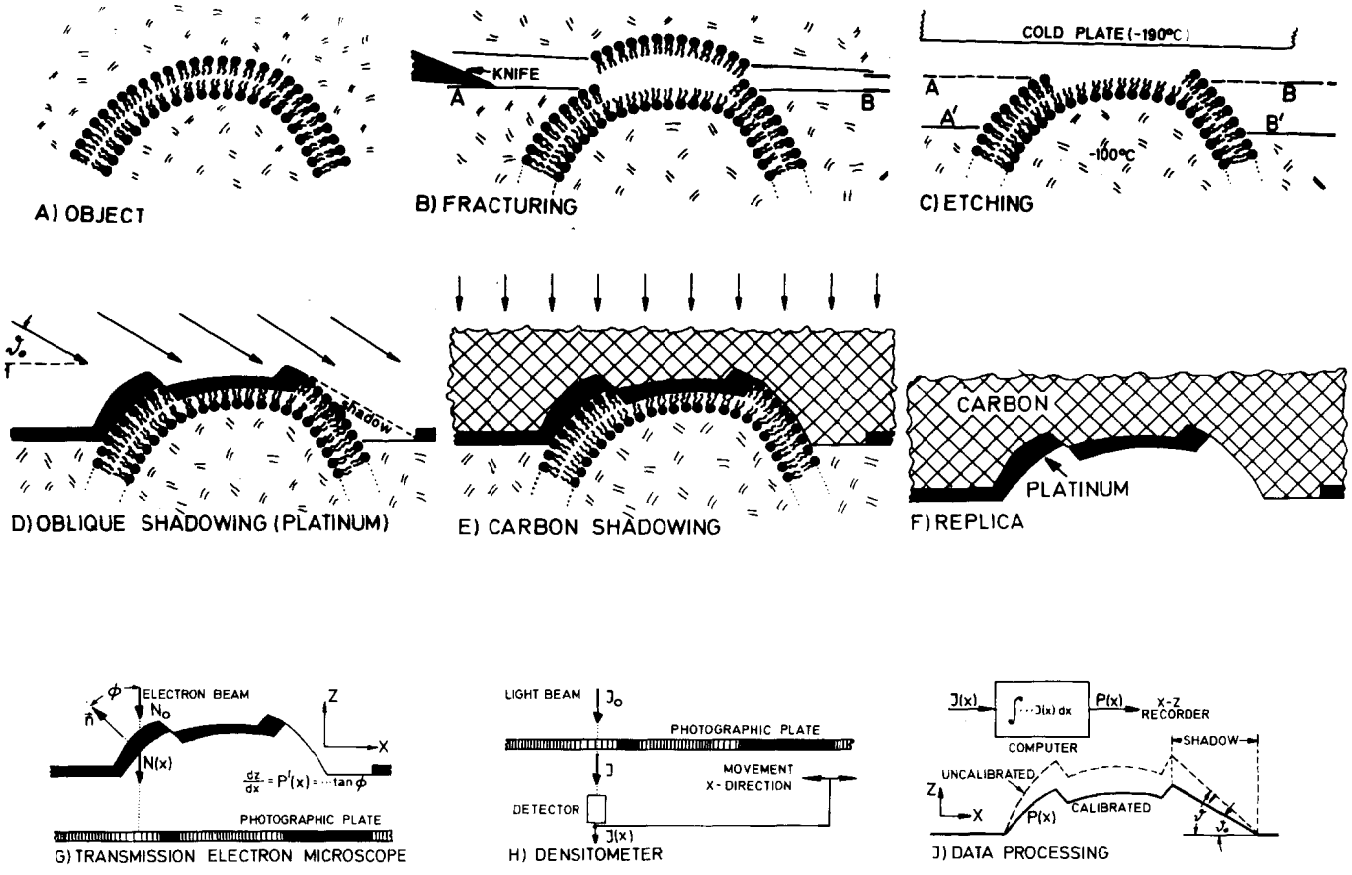

Fig. 1. Principle of the method. Schematic representation. A, Frozen object containing vesicle; B, fracturing: line AB defines cutting plane; C, etching: $A'B'$ defines water surface after etching procedure; D, oblique shadowing with heavy atoms (platinum); ϑ_0, shadowing angle; E, carbon shadowing leads to mechanically stable replicae; F, replicae containing the information of surface profile in terms of modulation of platinum film thickness. Organic material and water removed with chloroform. G, Photographic exposure procedure in the transition electron microscopy. z-axis defines direction of electron beam. n is the normal of an area element of the object. $P(x)$ is the profile of the object. H, evaluation of photographic plate by densitometer. I, upper part: correlation of densitogram $J(x)$ to surface profile $P(x)$. Lower part: dashed line gives measured profile. Thick line: calibrated profile obtained by equalizing ϑ_0 and ϑ.

10^5 degrees $\cdot$ s^{-1}. The cooling rates were determined by analysing the size of precipitations formed in water/glycerol mixtures [6]. The fracturing/etching technique was performed in a Balzers freeze etching device (BAF 301). First, the samples were cut in a microtome. This procedure exhibits the inner core of the bilayers (fracturing face, Fig. 1B). The outer surface was exposed by evaporation of the water to a depth of about 1000 Å (Fig. 1C).

The yeast cells were embedded in a water/glycerol mixture containing 2% glycerol. These samples were all frozen by the slow cooling technique.

Shadowing technique. The etched surfaces were shadowed with platinum/carbon with an oblique angle of $\vartheta_0 = 45°$. The layer thickness was 30 Å. The samples were covered with a carbon film of about 300 Å by shadowing in a direction normal to the cutting plane. According to Moor [7] the platinum/carbon compound gives the best resolution. When the shadowing procedure was accomplished the substrate was removed from the platinum/carbon layer with chloroform. The structure of the surface profile is stored in terms of the modulation of the thickness of the platinum film.

Picture analysis. The replicae were investigated with transmission electron microscopes. Sections of interest were photographed using a Dupont COS 7 film. These pictures were evaluated by recording absorbance along straight lines using a Nonius (CY 874 densitometer). The density values were stored in a Nicolet computer (B — NC 12) for further evaluation in terms of the surface profiles.

Principle of the method. The 3-dimensional reconstruction of the surface profile is based on an analysis of the platinum-film thickness. The latter is determined by measuring the absorption of the electron beam traversing the replica in a direction normal to the cutting plane (cf. Fig. 1G). The carbon film can be ignored since platinum has a much higher scattering cross section for electrons than carbon [8]. A complete description of the mathematical details of the method is given in the appendix. The basic idea is as follows: The path length ξ of the electron beam within the platinum film is related to its thickness, Δ, according to

$$\xi = \Delta \cos \Theta\,(x, y) = \Delta_0 \frac{\cos \Theta\,(x, y)}{\cos \phi(x, y)} \tag{1}$$

Δ is the film thickness in a direction parallel to the normal, n, of the membrane

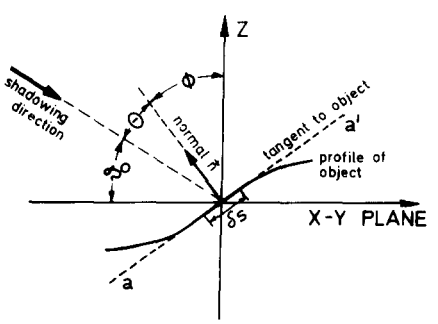

Fig. 2. Evaluation of the surface profile. The x-y plane is defined by the cutting plane, z-direction along electron beam. aa' is tangent to local surface element, δs, along section defined by densitometer recording.

surface. Θ is the angle between the normal n and the shadowing direction, ϑ_0, and ϕ is the angle between n and the direction of the electron beam (cf. Fig. 2). Δ_0 is the platinum film thickness for $\Theta = 0$. Now, the first derivative $dz(x)/dx$ of the surface profile $z(x)$ in any direction x is directly related to the path length ξ, since

$$\frac{dz}{dx} = P'(x) = \tan \phi(x) \tag{2}$$

If $\xi(x)$ is known, the surface profile $z(x) = P(x)$ is obtained from Eqn. 2 by integration. ξ can now be determined by measuring the density of the negative film. If an exponential law of electron absorption is assumed, the surface profile is finally given by (see appendix).

$$P(x) = A + Bx + C \int_0^x \ln \log J(x)\, dx \tag{3}$$

$J(x)$ is the light intensity measured by the densitometer detector (Fig. 1H). A, B and C are constant. A, does not influence the profile, $P(x)$, and can be ignored. The constants B and C are eliminated as described in the appendix. C is determined by a calibration procedure based on the measurement of the shadow lengths.

Application

In the following, the present method is applied to both artificial and biological membranes.

(1) Three-dimensional reconstruction of a vesicle

Fig. 3 shows a vesicle observed under different angles (±6°) in the electron

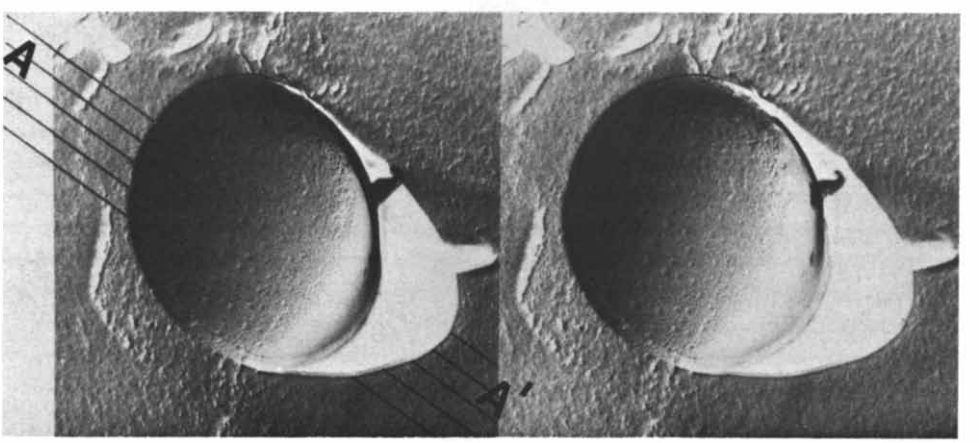

Fig. 3. Stereoscopic picture of a vesicle of a mixture of 65% dioleyl phosphatidic acid, 15% dioleyl phosphatidylcholine, 20% cholesterol. An impression of the three-dimensionality can be obtained by looking at the pictures with a pocket stereoscope (e.g. Zeiss TS4). It is found that the vesicle is curved towards the observer.

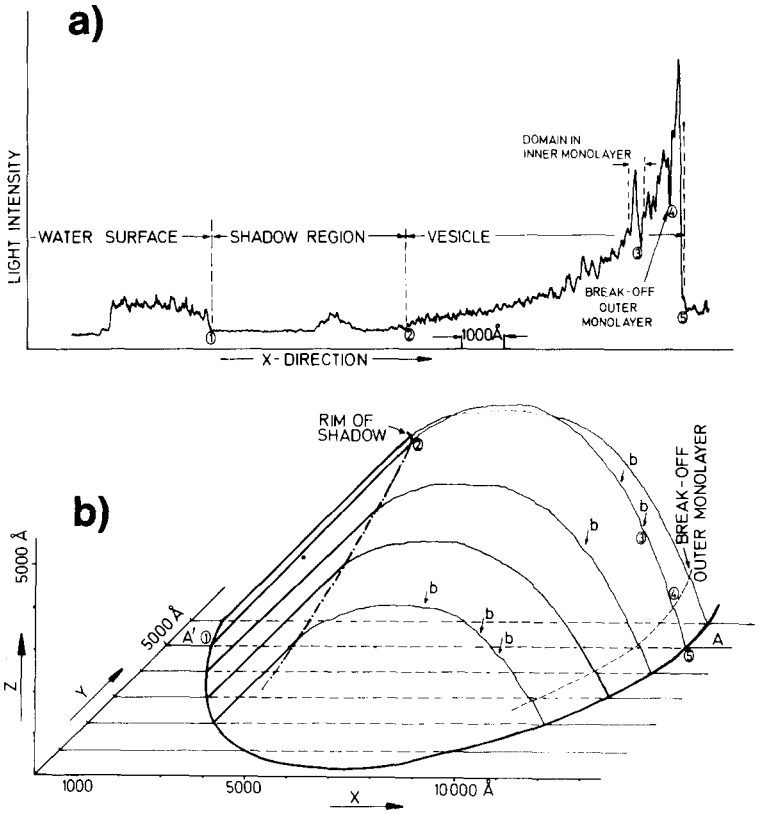

Fig. 4. Three-dimensional reconstruction of shape of vesicle showing Fig. 3. a, Densitometer curve along section AA' (cf. Figs. 3 and 4). Intensity I (cf. Fig. 1h) is given in arbitrary units. b, Five sections through vesicle (cf. Fig. 3 plotted in perspective. The thick drawn curve indicates the intersection of vesicle with cutting plane. Dashed line indicates the break-off of outer monolayer. Arrow b shows some domains formed by lateral phase separation.

microscope. In principle, the three-dimensional shape could be reconstructed by using appropriate instrumentation. The three-dimensional shape obtained by the present method is shown in Fig. 4. The calibrated surface profiles for several sections through the vesicles are shown. Calibration method (iii) was applied. In accordance with the stereoscopic picture a convex shape is observed. Our efforts to calibrate the surface profile $P(x)$ by using the stereoscopic pictures failed. The main reason is the difficulty to find the corresponding sections in the two pictures.

According to Eqn. A.11 it is evident that our analysis gives only reliable results to that point of the section where the shadow begins. Under ideal shadowing conditions a linear change in $P(x)$ between the beginning and the end of the shadow is expected since $J(x)$ = const in this region. In addition, the base lines on either side of the section should be at the same level. According to Fig. 4 the shadow region is neither linear nor are the base lines on the same level. Several reasons for this behaviour are possible which may not be separated. First, vagabond platinum atoms prevent the formation of an ideal shadow. Second, the absorption of the electron beam by the carbon film is

not negligible in the region of the platinum shadow. Third, relation A.8 is not valid at high electron densities (cf. Ref. 1 p. 250). Finally, Eqn. A.9 may be invalidated at high densities.

(2) Thickness of monolayers

An example of the usefulness of the method to determine fine structural features is also shown in Fig. 4. At the position marked by 4 there is a jump in the $P(x)$ curve. Comparison with the micrograph shows that at this position the outer monolayer has broken off. The height of the jump is a measure of the thickness of one monolayer. We obtain a value of $\delta = 26 \pm 3$ Å. This value is in good agreement with X-ray data yielding a membrane thickness of about 55 Å [9]. This high accuracy is reached by averaging over the coarseness of the platinum grains.

(3) Relation between molecular structure of lipid phases and surface profile fine structure

(a) Ripple structure. Fig. 5 shows the ripple structure [4,10—12] obtained upon cooling phosphatidylcholine at a temperature between the main- and the pretransition. Both the inner and the outer monolayer exhibit an arrangement of parallel dark and bright lines characterized by a well defined periodicity with wavelength Λ. Occasionally defects of characteristic symmetry (—, +) are seen (Fig. 5a). By analysing the symmetry of these defects together with the fine structure of the surface profile one may obtain information about the molecular structure of the lipid phase.

The surface profile $P(x)$ as obtained from the densitometer curve taken along the line $a\ b$ is given in Fig. 5b. It has the following characteristic features:

(i) $P(x)$ is periodic *

$$P(x) = P(x + \Lambda)$$

(ii) The surface profile $P(x)$ does not have an inversion center.

$$P(x) \neq -P(-x)$$

(iii) The defect symmetry leads to the conclusion (cf. Appendix and Ref. 4)

$$P(x) = P(-x)$$

(iv) The inner monolayer (P_i) exhibits the same surface profile as the outer one (P_o). The two profiles are shifted by $\Lambda/2$ in the x-direction and reflected at the xy-plane.

From these observations one can draw the following conclusion concerning

---

* As judged from Fig. 5a the periodicity seems to depend on the position of the vesicle. Clearly this variation in Δ is due to the fact that the electron micrograph is a two-dimensional projection to the plane AB (see Fig. 1c). However, the three-dimensional reconstruction shows that the ripple is really periodic. This example demonstrates that the dimensions obtained by visual inspection of the electron micrograph may be inaccurate. In Fig. 5a for instance, the 'periodicity' varies by a factor of two. This clearly demonstrates the advantage of the three-dimensional reconstruction procedure.

the molecular arrangement. From the assumption that the hydrocarbon chains compose most of the bilayer volume, it follows that the average chain axis is tilted with respect to the normal of the membrane surface. Without such a tilt the distortions expected at the maxima (M') and minima (M) would create too much free volume. This conclusion agrees with X-ray data [12—14] providing strong evidence that the chains are tilted in the ripple phase. A very characteristic feature of the ripple structure is its well-defined periodicity. Chain tilting alone could not explain this strong periodicity. One has to look for further contributions to the bilayer free energy. As shown previously [4] it is determined

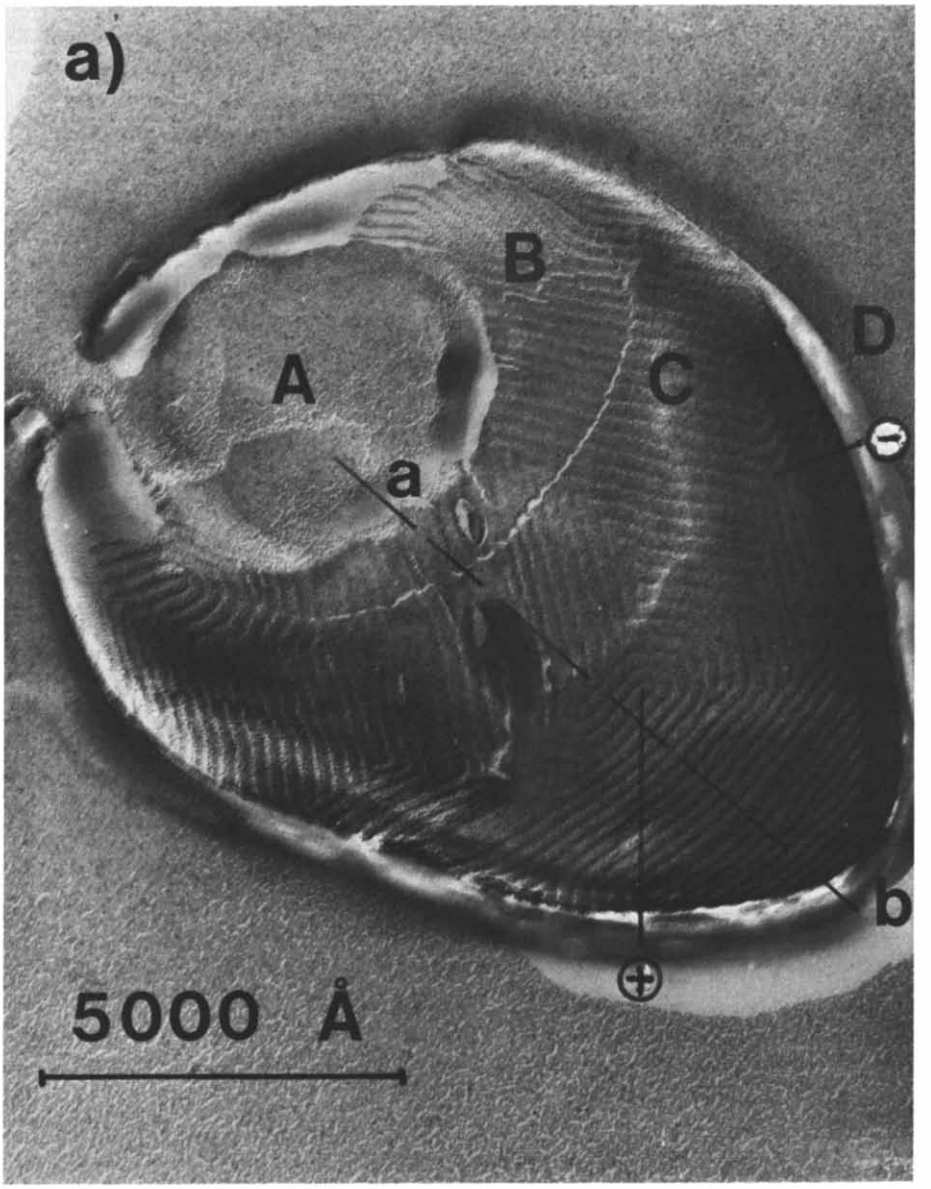

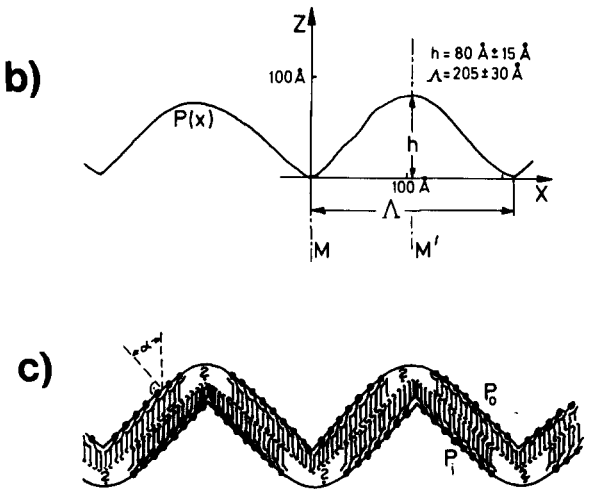

Fig. 5. (a) Micrograph of a large bilayer vesicle of dimyristoyl phosphatidylcholine as obtained upon cooling at a slow cooling rate from a temperature of 18°C. A = inner water phase, B = inner monolayer, C = outer monolayer, D = outer water phase. (b) Surface profile as obtained by three-dimensional reconstruction. Both M and M′ are mirror planes. (c) Model of deduced molecular lipid organization. Molecular tilt angle α with respect to local membrane normal.

by the following factors: (1) The gain in free energy by the spontaneous curvature of the monolayers, (2) the compression energy associated with a variation in membrane thickness leading to alternative regions of compression and dilatation and (3) interfacial energy at the maxima and minima. The spontaneous curvature is a natural consequence of the polar shape of the lipid molecule. It can only occur if the two opposing monolayers are decoupled. In the previous work [4] we could not predict the sign of the spontaneous curvature. It is the three-dimensional surface profile which gives information on both the sign and absolute value of the spontaneous curvature. At the maxima (M') the surface profile is rather flat. One even observes sometimes an inverse curvature in these regions. This is not easily explained by our model. According to Larsson, this flatness of the extrema could be explained by assuming that, there, the lipid molecules are non-tilted (Larsson, private communication and Ref. 14). However, this is in contradiction with the sharp edges observed at the minima (M).

A closer inspection of Fig. 5a shows that the profiles of faces B (inner monolayer) and C (outer monolayer) are different. This clearly demonstrates that the membrane thickness varies in a direction normal to the ripples. This leads to the conclusion that each monolayer rather then the whole bilayer exhibits a spontaneous curvature.

(b) Spiral structure. Fig. 6 shows a vesicle cooled from a temperature below the pretransition. At first sight the picture seems again to exhibit a wave-like pattern. However, a closer inspection as well as the three-dimensional picture analysis show the following essential differences as compared with Fig. 5a: (i) There is no periodicity on a large scale. (ii) The defects exhibit a spiral pattern. (iii) At the origin of the spiral the membrane exhibits a pronounced invagination. In some cases a conical cap is formed. (iv) The surface profile $P(x)$

differs considerably from that of the ripple structure (Fig. 5b). More precisely, $P(x)$ does not have a mirror plane ($P(x) \neq P(-x)$). This escape of the membrane in the third dimension was observed previously without picture analysis from inspection of the shadow distribution [4]. This latter finding led us to the conclusion that the membrane structure is biaxial due to a strong coupling between the monolayers. Although the spiral pattern is consistent with the biaxiality it

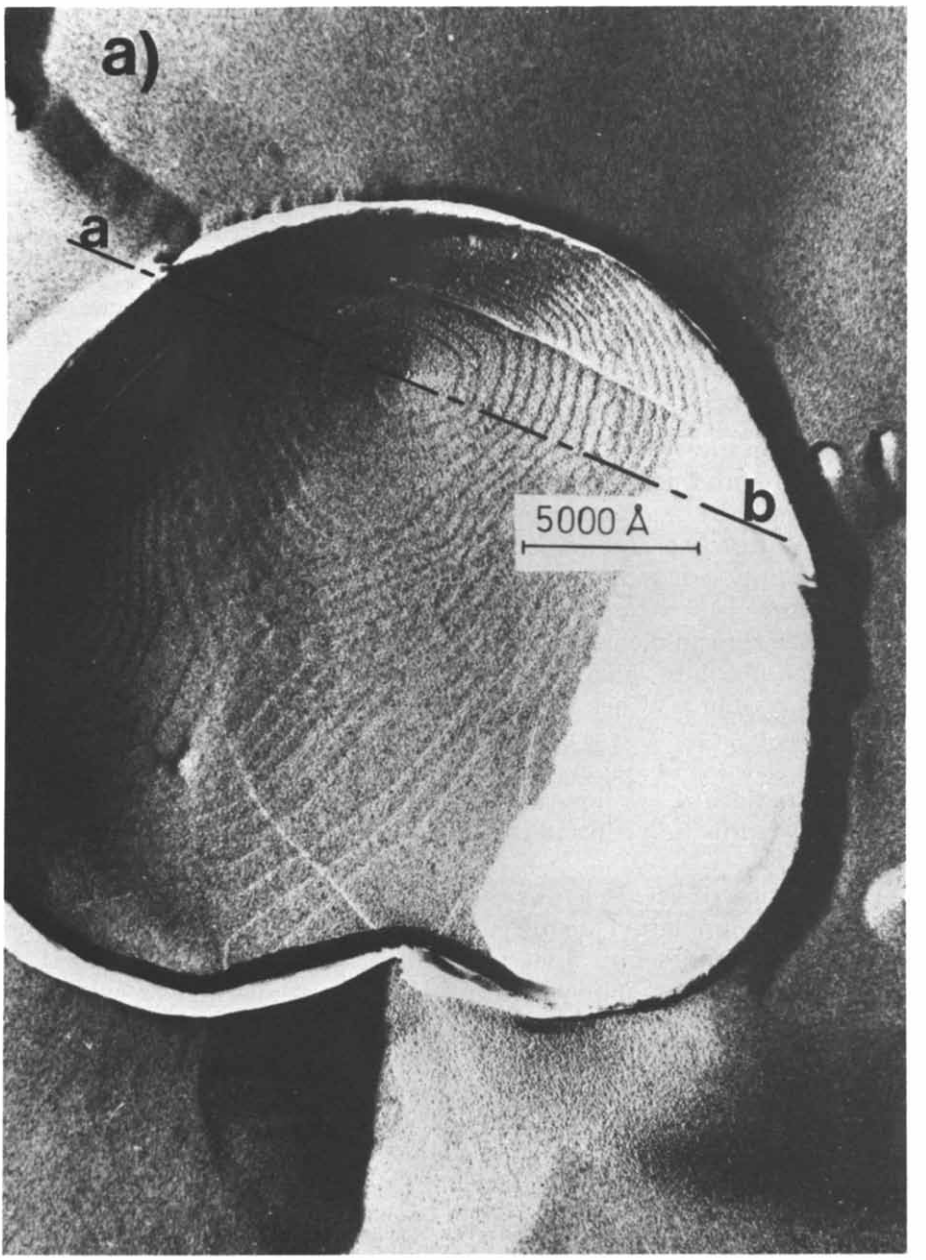

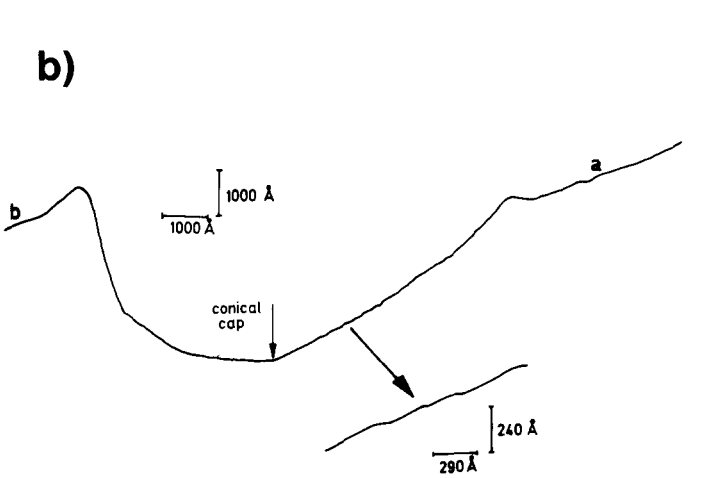

Fig. 6. (a) Micrograph of large bilayer vesicle of dimyristoyl phosphatidylcholine as obtained upon cooling from 4°C at a fast cooling rate immediately after decreasing the temperature below the pretransional point. (b) Surface profile as observed along the section a b.

is not necessarily a consequence of it. It may rather be caused by the growth kinetics of the defect structure.

(4) Domain structure of lipid alloys

Figs. 3 and 4 show a vesicle of a 3-component-lipid mixture. The electron micrograph (Fig. 3) shows that the surface is covered by small domains with diameters of several hundred Å. Since the domains show a shadow one can conclude that they differ in curvature from the bulk membrane surface. The three-dimensional structure of the domains may be accurately determined by recording density curves with high resolution. Fig. 7 shows an enlargement of the membrane surface profile in a region containing such a domain. Clearly, the change of the curvature at the boundary is rather smooth. The domain width, d, is defined by the distance of the points of inflexion (F_1, F_2). Judged from a visual inspection of the electron micrograph, the domains seem to have a much sharper boundary and the size can be considerably underestimated. This is due to the above mentioned fact that the electron micrograph is in reality the first derivative of the surface profile. This illustrates the advantage of the present method as a tool for quantitative analysis of membrane fine structure. In addition, the diameter of the domains and the average inter-domain distances can only be determined from the three-dimensional surface profile $P(x)$. The normal electron micrograph gives the two-dimensional projection of the domains.

The formation of stable domains has been explained as follows [4]: Each lipid component is characterized by a specific value of the spontaneous curvature [4,15]. It is this special feature of lipid layers which allows us to distinguish regions of different lipid composition by the freeze quenching technique. The surface profile in the region of the phase boundary is determined by two factors, one of which is the chemical potential difference between the two lipid phases. The second contribution is the elastic energy associated with the splaying of the hydrocarbon chains in the transition region between the two

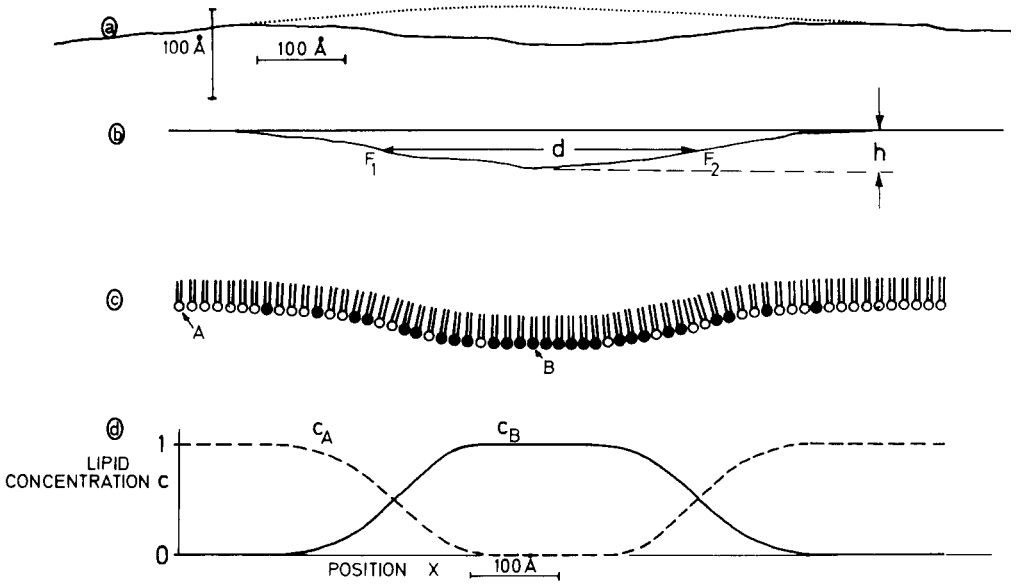

Fig. 7. (a) Enlargement of surface profile $P(x)$ of circular domain b in inner monolayer of the vesicle shown in Fig. 4. (b) Profile of domain after subtraction of overall curvature of the vesicle. The diameter d is given by the distances of the inflexion points F_1, F_2 (d = 350 Å). The height, h, is 38 Å. (c) Schematic molecular arrangement of the two lipid components in the domain region. (d) Lipid composition suggested by smooth variation in surface curvature at the phase boundary.

components. The distribution of the lipid components is adjusted in such a way that the total free energy of the above mentioned contributions is minimized. The smooth variation in surface curvature at the phase boundary provides strong evidence that the lipid composition also varies smoothly in this region.

Fig. 7 shows an example of domains of the inner monolayer which are all bent towards the inside of the vesicle. The domains of the outer monolayer are all bent in the opposite direction. The possibility that the inner and outer monolayers are coupled together in such a way that they are both bent towards the same side can be excluded. Otherwise one would expect that the domains in one monolayer should be bent towards either side.

As judged from the typical findings in three-dimensional alloys, one would expect that the domains coalesce into larger regions by the well-known coarsening process [16]. This would be the case if the free energy of the phase boundary was dominated by the chemical potential. It is the elastic force field associated with the observed variation in surface curvature at the phase boundary which provides a repulsive force between the domains and which thus stabilizes the domain structure. By taking into account such considerations, the domain size can be estimated [4].

(5) Charge induced domain structure [17,18]

In previous spectroscopic work it was shown that external charges such as Ca^{2+} or charged proteins may induce lateral phase separation in lipid layers composed of charged and uncharged lipids [17]. The phase separation is caused by the interaction of the external charged particles with the charged lipid com-

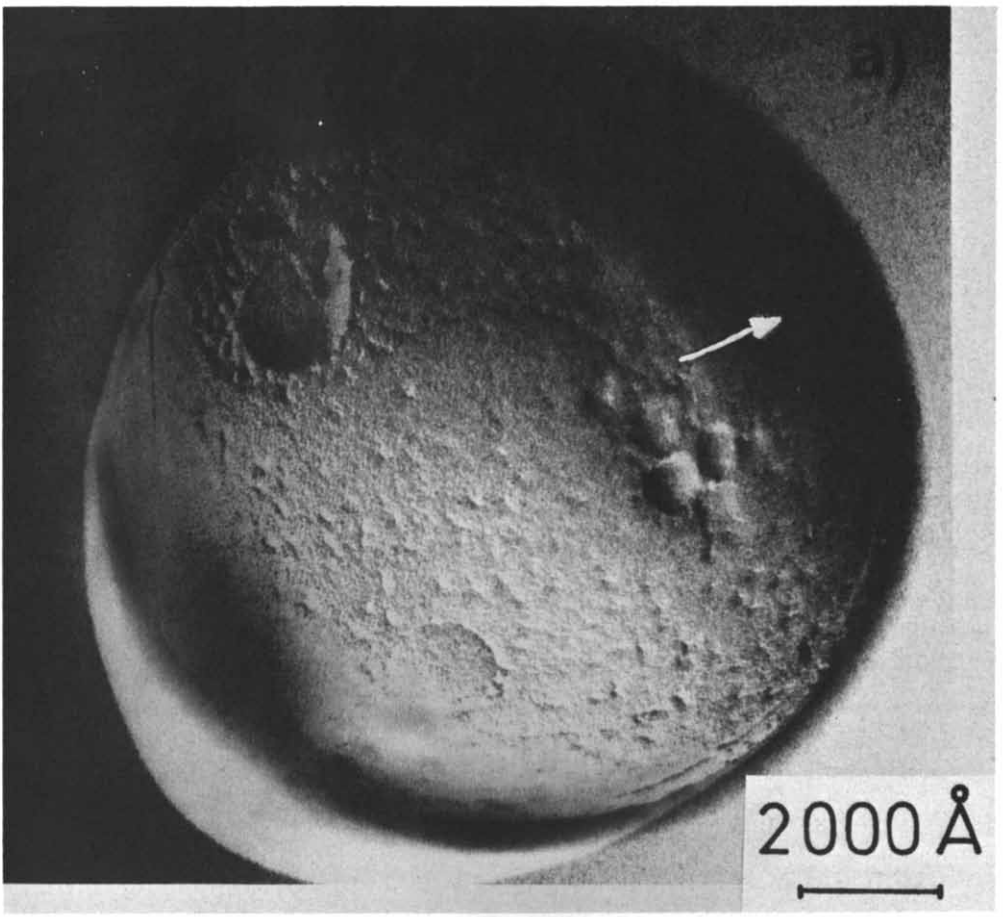

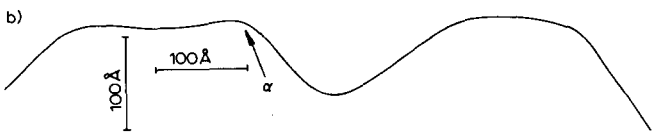

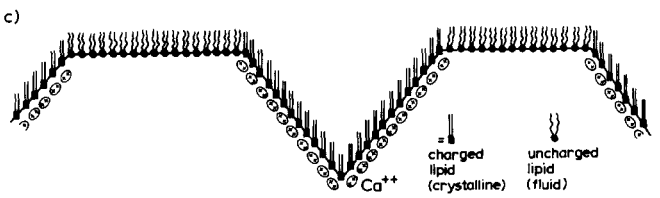

Fig. 8. (a) Ca^{2+}-induced domain structure in 1 : 1 mixture of dioleyl phosphatidylcholine and dioleyl phosphatidic acid. Frozen from 20°C at slow cooling rate [17]. Arrow indicates that the base of the domain is of deltoid shape. (b) Surface profile $P(x)$ of Ca^{2+} induced domain. (c) Molecular model as suggested by triangular surface profile.

ponent. It is seen in Fig. 8a that the phase separation leads to a domain like organization of charged and uncharged lipids.

Fig. 8a shows an electron micrograph of a vesicle composed of a 1 : 1 mixture of dioleyl phosphatidylcholine and dioleyl phosphatidic acid after addition of Ca^{2+}. Clearly the surface is covered by a large number of sharp edged domains. The spectroscopic work suggests that these domains have to be attributed to Ca-bound charged lipid. Due to the Ca-binding, the lipid has undergone a transition to the crystalline state. The three-dimensional picture analysis is a good tool in order to determine both the size distribution of the domains and the crystallographic structure. The basic observations are:

(i) The bases of the domains exhibit a pronounced deltoid contour (cf. Fig. 8a arrow). This suggests that the Ca^{2+}-bound charged lipid is in a crystalline state which is in complete agreement with the spectroscopic result [17].

(ii) The surface profile exhibits a nearly triangular shape. This provides strong evidence that the Ca^{2+}-bound charged lipid is tilted, that is in a biaxial phase. It is interesting to notice that according to Fig. 8b the surface curvature at the boundary of the domains does not change abruptly (cf. Fig. 8b arrow α). This indicates also a smooth variation in composition at the boundary. As mentioned above this is due to a relaxation in elastic strain at the phase boundary. A direct consequence of this relaxation is a repulsive force between the domains which prevents the coarsening process.

(6) Lateral organization of biological systems

It is well known that biological membranes are organized in a heterogeneous way both with respect to the distribution of lipids and proteins within the plane of the membrane (lateral organization) and between the two monolayers (inside-outside organization). This heterogeneous structure of membranes can be directly observed by freeze etching microscopy. As an example Fig. 9 shows an electron micrograph of the inner and outer membrane face of yeast cells. Two outstanding structures are visible:

(i) In the outer face a regular arrangement of particles is observed (cf. Fig. 9a arrow). These patches of particles are rather flat.

(ii) Other regions of high particle density are seen in both faces which are characterized by a very elongated damlike shape. The particles exhibit a random lateral distribution. Fig. 10a shows an enlargement of the damlike regions. In Fig. 10b the surface profile is shown in a direction perpendicular to the long axis. The relatively large height of the dams shows that the particle assemblies induce a very strong variation in membrane curvature. The most interesting feature, however, is that the high particle density is restricted to the top of the dam-like regions, whereas the slopes are nearly particle-free. Obviously, the particle assembly leads to a change in curvature which extends very far into the lateral direction perpendicular to the long axis. As shown previously, such far-reaching distortions of lipid bilayers may be caused by protein binding combined with a spontaneous curvature of the membrane [19,20].

The method of three-dimensional reconstruction of surface profiles may also be used in order to distinguish between different membrane bound proteins. Such an application of the method is shown in Fig. 10. The surface profiles of several proteins were determined. At least two types of proteins could be

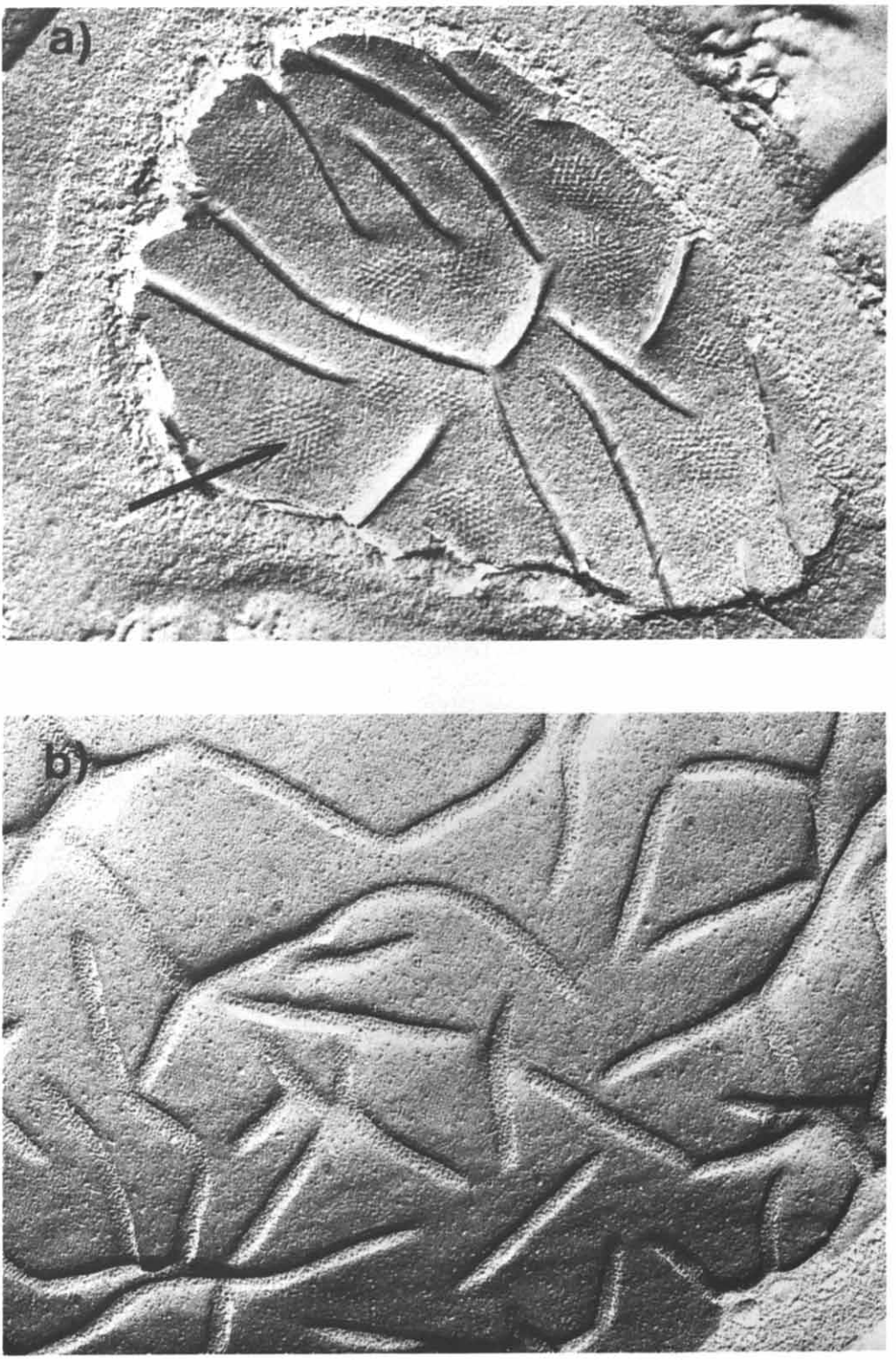

Fig. 9. Electron micrograph of slowly cooled yeast cells in a glycerol/water mixture. (a) Outer membrane face; (b) inner membrane face.

distinguished by the shape of the surface profile. These profiles, $P(x)$, are shown in Figs. 10c and 10d:

(i) The first type of protein (I) (cf. Fig. 10c) is characterized by a relatively flat and extended shape of $P(x)$ (ratio height to width $h_I/d_I \approx 0.65$). It is more often found within the slope area of the dam-like protrusion rather than within the flat membrane region. Most probably it is this type of protein which occupies the tops of the dams. The rather large value of the width d_I ($\approx 52 \pm 10$ Å) suggests that the lateral extension of the type I protein is determined by two factors. First, the intrinsic lateral dimension of the protein and secondly the protein induced distortion of the lipid layer. This conclusion is verified by the rather smooth variation in curvature at the transition from the protein to the membrane. This type of protein could not be characterized in terms of its extension by simple visual inspection (Fig. 10a).

(ii) The second type of protein II (cf. Fig. 10d) is characterized by a much larger amplitude-to-width ratio ($h_{II}/d_{II} \approx 2.8$). The shape, $P(x)$, of the type II protein exhibits a steep slope and is characterized by an abrupt transition into the undistorted membrane region.

Discussion of the method

The examples presented above have shown that the method proposed in the present paper is well suited to reconstruct three-dimensional surface profiles of membranes and may be used to characterize membrane bound particles.

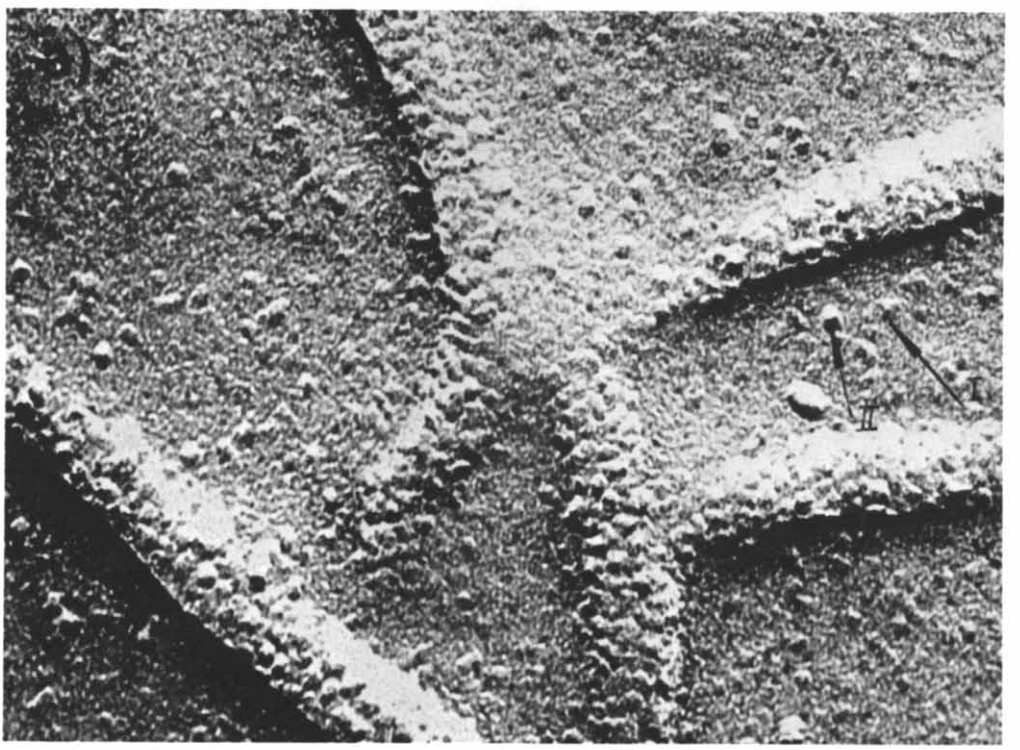

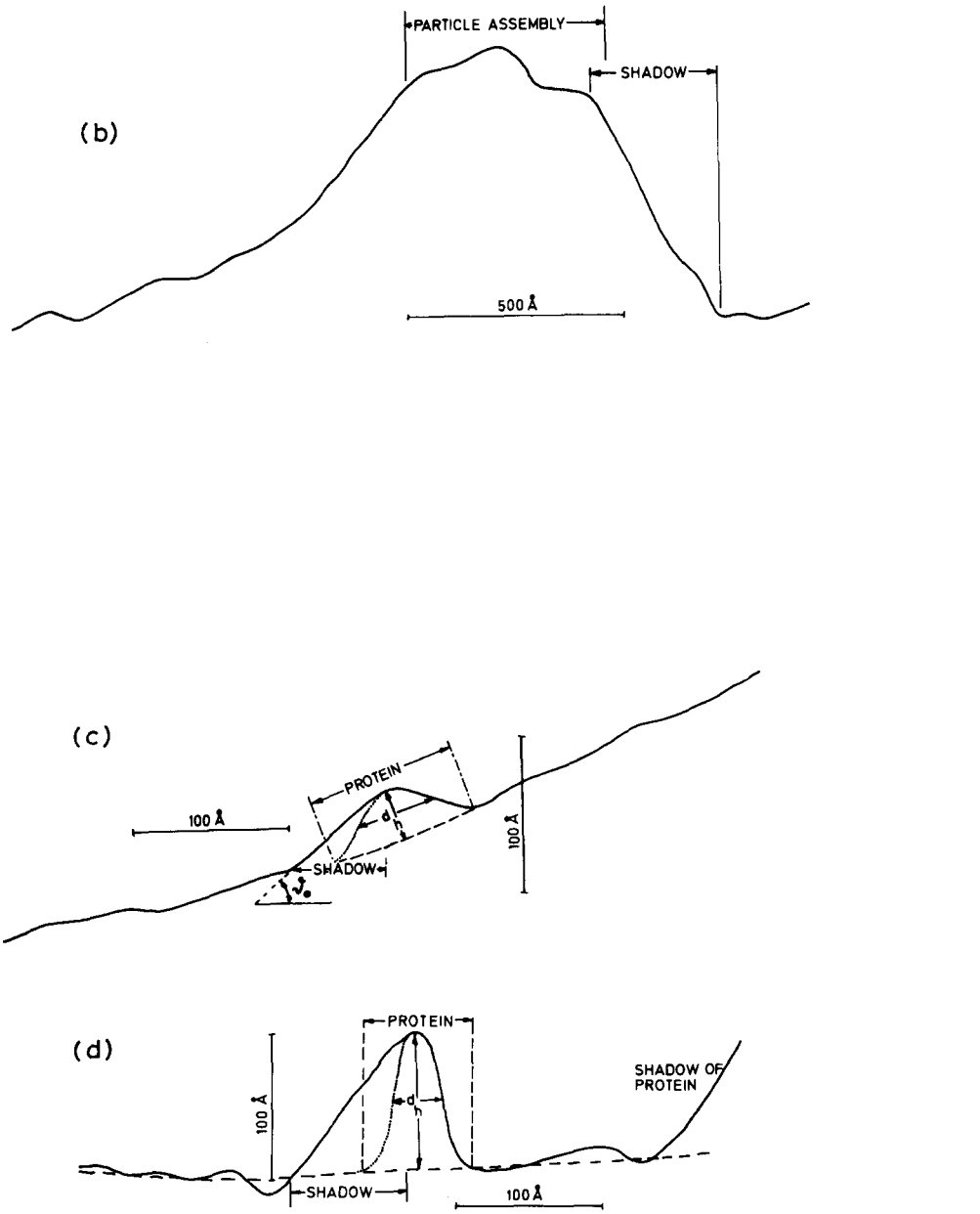

Fig. 10. (a) Enlarged electron micrograph of Fig. 9b. (b) Surface profile $P(x)$ in a direction perpendicular to the long axis of the dam-like patches. (c) Surface profile $P(x)$ of type I particle. Ratio of height to width $h/d \approx 0.65$. (d) Surface profile $P(x)$ of type II particle. $h/d \approx 2.8$. Particles I and II are indicated by arrows in Fig. 10a.

The resolving power of the method depends (i) on the size of the platinum grains and (ii) on the diameter of the densitometer light beam. At large electron microscope magnifications the resolving power is determined by the platinum grain size alone. It varies between 10 and 20 Å. The accuracy in measuring transversal steps in the membrane may be better than the grain size since one

performs an averaging process upon recording the densitometer curves. Therefore it was possible to determine the monolayer thickness to an accuracy of 3 Å. Since the orientation of the cutting plane is not known exactly, the absolute heights can only be determined to an accuracy of about 20%.

The method described in the present paper applies for densitograms recorded in a direction parallel to the shadowing direction. The method may of course also be applied for other directions. In principle it may also be used if the rotating shadowing technique is applied. With this technique more information could be obtained about the lateral dimension and the shape of the surface profile. As a further approximation we assumed a linear relationship between film blackness and electron beam intensity. This source of error could be circumvented by making appropriate corrections for high electron beam intensities.

The power of the present method for structure research of model membranes has been demonstrated for several examples. It was shown that it provides the possibility to examine theoretical models of membrane structure. Thus, a previous model of the ripple structure based on the idea of a spontaneous curvature of the lipid monolayer [4] was verified with this technique. The three-dimensional reconstruction technique allows determination of true distances over a large extension of macroscopically curved systems such as vesicles or cells, whereas the normal, visual inspection of electron micrographs gives only projection of distance onto the cutting plane. The proposed method allows a statistical evaluation of particle sizes and inter-particle distances and thus opens the possibility to develop molecular statistical models of small multicomponent systems such as vesicles and cells.

In studies of biological membranes, the conventional method of freeze etching microscopy gives essentially a qualitative picture of the structure. The present method opens the possibility of quantitative structural studies. Both the height and the lateral dimensions of membrane bound particles may be determined. Thus molecular weights may be estimated. Since small variations in curvature may be observed it is possible to study also distortions of lipid layers induced by the incorporation of macromolecules. From such studies models of long-range particle interaction may be developed [20]. Other examples of application are, the quantitative analysis of cell surface modulation by drugs or mitogenic substances.

Appendix

Reconstruction of 3-dimensional surface profiles. In the following we derive a relationship between the thickness of the platinum film and the surface profile. The calculation involves several steps.

(1) The platinum film thickness, Δ, measured in a direction perpendicular to the surface, is related to the angle Θ between the shadowing direction, ϑ_0, and the normal n of the local surface element according to (cf. Fig. 2)

$$\Delta = \Delta_0 \cdot \cos \Theta \qquad \text{(A1)}$$

Δ_0 is the maximum thickness obtained for $\Theta = 0$.

(2) The effective path length, ξ, of the electron beam within the platinum

layer depends on this film thickness Δ and the angle ϕ (cf. Fig. 2) in the following way

$$\xi = \frac{\Delta}{\cos \phi} \tag{A2}$$

According to Fig. 2, the angles ϑ_0, Θ and ϕ are related by the following equation

$$\Theta = 90° - \phi - \vartheta_0 \tag{A3}$$

Combining Eqns. A1, A2 and A3 yields

$$\xi = \Delta_0 \{\cos(90° - \vartheta_0) + \sin(90° - \vartheta_0) \cdot \tan \phi\} \tag{A4}$$

(3) The basic relation between the local slope of the object and the angle ϕ is

$$\frac{dz}{dx} = P'(x) = \tan \phi(x) \tag{A5}$$

where $P(x)$ is the function describing the surface profile along the section defined by the densitometer. Inserting $\tan \phi(x)$ from Eqn. A4 the surface profile $P(x)$ is given by

$$P(x) = \text{const} + \int_0^x \left\{ \frac{\xi(x)}{\Delta_0 \cdot \sin(90° - \vartheta_0)} - \cot(90° - \vartheta_0) \right\} dx \tag{A6}$$

(4) Now, it is assumed that the attenuation of the electron intensity by the replicae is completely described by an exponential absorption law

$$N(x) = N_0 \cdot e^{-\alpha \cdot \xi(x)} \tag{A7}$$

In this equation, N_0 is the current density of the incident electron beam, while $N(x)$ is the current density of the electron beam (cf. Fig. 1G) passing through position x_0. α is the absorption coefficient. It may be a complicated function of absorption and incoherent scattering processes. As shown below, it can be eliminated by a calibration procedure.

(5) The absorbance of the photographic plate is proportional to the number of electrons entering the plate during the exposure time T_{ex} (Ref. 1, p. 249)

$$S(x) = a' \cdot T_{ex} \cdot N(x) = N(x)/a \tag{A8}$$

Such a linear relationship is only valid for $S(x) < 0.2\, S_{max}$, where S_{max} is the maximum absorbance of the photographic plate (Ref. 1, p. 250).

(6) Now, $S(x)$ is measured in the densitometer according to

$$S(x) = \log \frac{J_0}{J(x)} \tag{A9}$$

J_0 is the primary light intensity and $J(x)$ is the intensity of the light after passage through the photographic plate (cf. Fig. 1H). Combining A7, A8 and A9 yields

$$\xi(x) = \frac{1}{\alpha} (\ln \log J(x) - \ln \frac{a}{N_0} - \ln \log J_0 \tag{A10}$$

By inserting Eqn. A10 into A6 one obtains the final expression for the sur-

face profile $P(x)$

$$P(x) = A + B \cdot x + C \cdot \int_0^x \ln \log J(x)\, dx \qquad \text{(A11)}$$

where $B = -\left\{C\left(\ln \frac{a}{N_0} + \ln \log J_0\right) + \cot(90° - \vartheta_0)\right\}$

$$C = \frac{1}{\alpha \Delta_0} [\sin(90° - \vartheta_0)]^{-1}$$

The constant A does not determine the shape of $P(x)$ and can be ignored in the following. The integration in Eqn. A11 is performed by the computer. The baseline of $P(x)$ should be parallel to the plane $A'B'$ in Fig. 1C. However, the curve obtained after integration is tilted since B is not known. This tilt can be eliminated if a large enough section of the replicae is evaluated by the densitometer and if this section is parallel to the average plane $A'B'$.

A severe problem is the determination of the constant C. This can be overcome by a calibration procedure based on the measurement of the shadow length (cf. Fig. 11). Three methods are possible:

(i) First, the height of a sharp protrusion is determined from the shadow length L (cf. Fig. 11) and the shadow angle ϑ_0

$$H = L \tan \vartheta_0 \qquad \text{(A12)}$$

Then the protrusion is evaluated by the densitometer procedure which gives an apparent height H'. Finally the constant C is determined according to $C = H/H'$.

(ii) A second procedure can be applied if a section of the considered object has a nearly circular shape (cf. Fig. 11b). The circle of the section is unambiguously determined by the three points S, S' and T. A calibration equation is

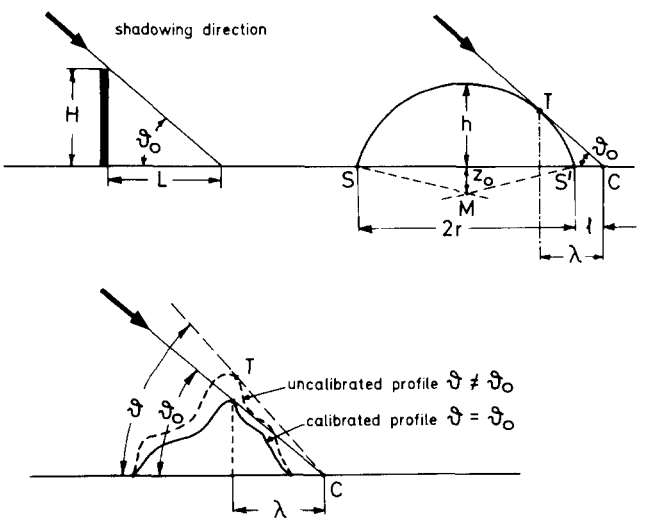

Fig. 11. Schematic representation of calibration procedure based on measurements of the shadow lengths L or λ, respectively, and the knowledge of the shadowing direction ϑ_0.

easily established for a shadowing angle ϑ_0 of 45° ($\tan \vartheta_0 = 1$). According to Fig. 11b

$$h = \sqrt{Z_0^2 + r^2} - Z_0 \tag{A13}$$

The unknown Z_0 can be determined from the condition that the straight line CT is tangent to the circle. A simple calculation yields

$$Z_0 = -(r + l) + \sqrt{2(r + l)^2 - 2r^2} \tag{A14}$$

In analogy to the first procedure the constant C is determined by equalizing the heights h' obtained from the densitometric analysis with the value of h from Eqns. A13 and A14.

(iii) For more complicated profiles the calibration can not be performed in a an analytic way. However, an iterative procedure can be applied in the following way: a straight line with slope $\tan \vartheta_0$ is drawn in such a way that it goes through the end point of the shadow C. Then the curve obtained by the densitometric procedure is varied in height until it touches the straight line at the point T. This iterative procedure can be easily incorporated in the computer program.

At this point it should be emphasized that it is the calibration procedure based on the absolute measurement of the shadow length which gives the information on the third dimension of the object. In this respect the method is closely related to the procedure of Eratostenes [3] for the determination of the earth radius.

Inspection of Eqns. A4 and A5 shows that the contrast of the pictures obtained by freeze etching methods is determined by the first derivative of three-dimensional surface structure. Accordingly, visual inspections of electron micrograph may give a rather false impression even in cases where three-dimensional pictures are observed by stereo methods. In particular considerable errors may occur in estimations of the lateral extensions of smoothly curved objects such as shown in Fig. 7 and Fig. 10c.

Acknowledgements

The electron microscopy experiments were performed in the Sektion für Elektronenmikroskopie at the University of Ulm. We are most grateful to Prof. R. Martin for his generous help. One of us (C. Gebhardt) would like to express his thanks to the Lucas Meyer Company, Hamburg, for a fellowship. Finally we thank the Deutsche Forschungsgemeinschaft for the financial support (under contract No. Sa 246 and Gr 551).

References

1 Reimer, L. (1967) Elektronenmikroskopische Untersuchungs- und Präparationsmethoden, p. 262, Springer, Berlin
2 Reimer, L. and Pfefferkorn, G. (1977) Raster-Elektronenmikroskopie, p. 221, Springer, Berlin
3 F.A. Brockhaus 1974, Wiesbaden, Enzyklopädie, Vol. 5, p. 619
4 Gebhardt, C., Gruler, H. and Sackmann, E. (1977) Z. Naturforsch. 32 c, 581—596
5 Bachmann, L. and Schmitt-Fumian, W.W. (1973) Freeze-Etching Techniques and Applications (Benedetti, E.L. and Farvard, P., eds.), Chapt. 7, Soc. Franc. de Microscopie Electr., Paris

6 Van Venrooij, G.E.P.M., Aertsen, A.M.H.J., Hax, W.M.A., Ververgaert, P.H.J.T., Verhoeven, J.J. and van der Vorst, H.A. (1975) Cryobiology 12, 46—61
7 Moor, H. (1971) Phil. Trans. R. Soc. Lond. B., Biol. Sci. 261, 121—131
8 Marmier, P. (1968) Kernphysik I, p. 61, VMP, Zürich
9 Chapman, D., Williams, R.M. and Ladbrooke, D.D. (1967) Chem. Phys. Lipids 1, 445—475
10 Verkleij, A.J., Ververgaert, P.H.J., van Deenen, L.L.M. and Elbers, P.F. (1972) Biochim. Biophys. Acta 288, 326—332
11 Janiak, M.J., Small, D.M. and Shipley, G.G. (1976) Biochemistry 15, 4575—4580
12 Luna, E.J. and McConnell, H.M. (1977) Biochim. Biophys. Acta 466, 381—392
13 Tardieu, A., Luzzati, V. and Reman, F.C. (1973) J. Mol. Biol. 75, 711—733
14 Larsson, K. (1977) Chem. Phys. Lipids 20, 225—228
15 Helfrich, W. (1973) Z. Naturforsch. 28c, 693—703
16 Haasen, P. (1974) Physikalische Metallkunde, Springer, Berlin
17 Galla, H.J. and Sackmann, E. (1975) Biochim. Biophys. Acta 401, 509—529
18 Hartmann, W., Galla, H.J. and Sackmann, E. (1977) FEBS Lett. 78, 169—172
19 Gruler, H. (1975) Z. Naturforsch. 30c, 608—614
20 Gruler, H. and Sackmann, E. (1977) Croatica Chem. Acta 49, 379—388